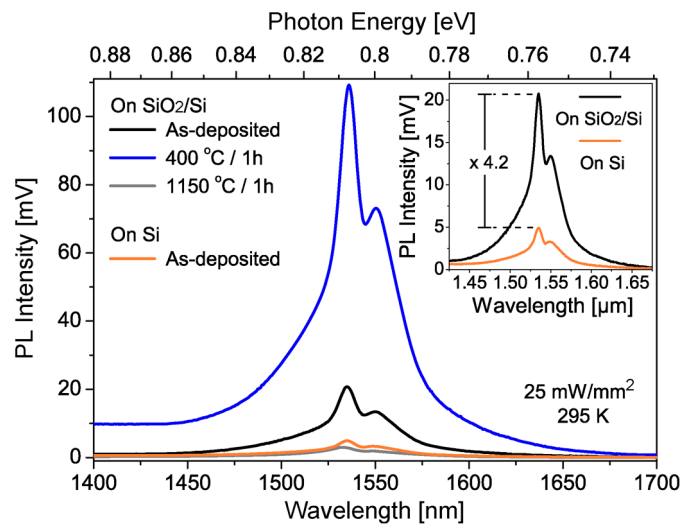


Highly Luminescent a-SiO_x<Er>/SiO₂/Si Multilayer Structure

Volume 4, Number 4, August 2012

Rossano Lang
David S. L. Figueira
Felipe Vallini
Newton C. Frateschi



DOI: 10.1109/JPHOT.2012.2204239
1943-0655/\$31.00 ©2012 IEEE

Highly Luminescent a-SiO_x<Er>/SiO₂/Si Multilayer Structure

Rossano Lang, David S. L. Figueira, Felipe Vallini, and Newton C. Frateschi

Device Research Laboratory, Applied Physics Department, “Gleb Wataghin” Physics Institute, University of Campinas—UNICAMP, 13083-859 Campinas SP, Brazil

DOI: 10.1109/JPHOT.2012.2204239
1943-0655/\$31.00 © 2012 IEEE

Manuscript received May 10, 2012; revised June 5, 2012; accepted June 6, 2012. Date of publication June 11, 2012; date of current version June 28, 2012. This work was partially supported by the Brazilian financial agencies CNPq and FAPESP through the National Institute for Science and Technology in Optics and Photonics (FOTONICOM). Corresponding author: N. C. Frateschi (e-mail: fratesch@ifi.unicamp.br).

Abstract: We have fabricated highly luminescent samples with erbium-doped amorphous silicon suboxide (a-SiO_x<Er>) layers on SiO₂/Si substrates. The layers are designed to provide a resonance with large modal overlap with the active material and with low quality factor (Q-factor) at 1540 nm. Also, the structure has higher Q-factor resonances in the wavelength range between 800 and 1000 nm. Within this range, strong light emission from a-SiO_x defect-related radiative centers and emission from the Er³⁺ ⁴I_{11/2} – ⁴I_{15/2} optical transition (980 nm) are observed. A twofold and fourfold improvement in photoluminescence (PL) intensity are achieved in the wavelength ranges between 800 and 1000 nm and between 1500 and 1600 nm (region of Er³⁺ ⁴I_{13/2} – ⁴I_{15/2} transition), respectively, when compared to the a-SiO_x<Er> active material deposited directly on Si substrate. The latter higher PL intensity enhancement is apparently caused by optical pumping at 980 nm (higher Q-factor) with subsequent emission from the ⁴I_{15/2} level in the low Q-factor resonance at 1540 nm. Further, five times increase of this emission at 1540 nm is obtained after optimized temperature annealing. The temperature-induced quenching in the PL intensity indicates distinct deactivation energies related to different types of Er centers which are more or less coupled to defects depending on the thermal treatment temperature

Index Terms: Photonics materials, optical properties of photonics materials, oxide materials.

1. Introduction

Numerous attempts toward obtaining gain or employing Si as an active medium for direct application in optoelectronics devices have been reported [1]–[3]. However, this task has been shown to be difficult and several alternatives have been proposed, such as hybrid integration with III–V alloys [4], Si nanocrystals formation in amorphous Si matrices [5] and Raman amplification [6]. In this context, erbium-doped silicon-based materials have been recognized as attractive and promising for telecom applications due to the luminescence originated from the transition between the Er³⁺ two lowest spin-orbit levels (⁴I_{13/2} – ⁴I_{15/2}) that occurs at 1540 nm, the C-band center.

In an amorphous Si matrix, the Er³⁺ excitation mechanism is associated to a defect-related Auger quaresonant process (DRAE) involving dangling bonds states and the Er³⁺ ground state [7] and/or a resonant dipole-dipole interaction originated by the nonradiative recombination of the electron-hole pairs in dangling bonds [8]. In both cases, electrons of the 4f shell are excited from the ⁴I_{15/2} to the ⁴I_{13/2} level. It has also been suggested a direct pumping of the ⁴I_{11/2} level by either tail-to-tail states recombination, a similar mechanism as above, or by up conversion caused by Er–Er

interaction [9]. However, a much more efficient approach to populate the $^4I_{11/2}$ level is by external optical pump at 980 nm such as in Er-doped fiber amplifiers (EDFAs) [10]. The electrons decay nonradiatively to the $^4I_{13/2}$ level and provide gain to the $^4I_{13/2} - ^4I_{15/2}$ transition. Another way, less frequently used, is via the $^4I_{15/2} - ^4I_{9/2}$ transition at 807 nm [11]. This transition has a small optical absorption cross section (typically on the order of $10^{-21} - 10^{-20} \text{ cm}^2$, depending on the host material) [12]. For this reason, there is significant interest in sensitizing Er³⁺ ions by adding strongly absorbing elements that can efficiently transfer energy to Er [13]. From this point of view, some reports have shown evidence of the direct energy transfer from silicon nanocrystals (Si-NC's) to Er³⁺ through nonradiative recombination of excitons [14], [15]. However, Kuritsyn *et al.* argued that Si-NC's embedded in silicon oxide are not specific in any respect when compared to other types of defects due to excess silicon; and a noteworthy defect-mediated and resonant optical excitation of Er³⁺ was verified [16]. We have demonstrated an enhancement of the emission at 1540 nm when erbium-doped amorphous silicon suboxide (*a*-SiO_x(Er)) layers with embedded Si-NC's were properly placed in vertical low quality factor (Q-factor) multilayer structure [17]. However, high temperature annealing such as 1000 °C required for the Si-NC's formation, has given rise to a strong deterioration of the Er³⁺ emission at 1540 nm when compared to the material annealed at lower temperatures [17].

Since the spontaneous emission in this material is low, several methods have been proposed for its enhancement. For instance, this can be achieved by increasing the optical mode confinement in the active region and hence, increasing the Purcell factor. Recent works have demonstrated spontaneous emission enhancement using the known high optical mode confinement provided by slot waveguides, particularly, in Er-doped SiO₂ waveguide structures [18], [19]. In other materials and/or structures, such as nitride-based light-emitting diodes, surface plasmons have been used to increase the photonic density of states thereby resulting in an enhance of the spontaneous emission rate [20], [21]. In principle, this approach may be used for the Er-doped material presented here. In this paper, instead of employing Si-NC's for electronic excitation transfer to the Er ions, we have optimized the annealing temperature to enhance the emission in a broad wavelength range (800–1000 nm). This emission provides the optical pumping at 980 nm which is enhanced by a resonance near this wavelength. The pumping at 980 nm leads to emission at 1540 nm that is extracted from the structure through a low Q-factor, hence, high external quantum efficiency resonance. Essentially it is created a cross pumping mechanism. The emission in the 800–1000 nm wavelength range is mostly provided by optically active defect centers from the *a*-SiO_x matrix. It is important to observe that there is a considerable spectral overlap between the intrinsic *a*-SiO_x optical emission and the transition energies from the Er³⁺ $^4I_{15/2}$ level to the $^4I_{9/2}$ (1.536 eV–807 nm) and $^4I_{11/2}$ (1.265 eV–980 nm) levels. The vertical resonant structure consists of an *a*-SiO_x(Er) layer deposited on a SiO₂ layer thermally grown on Si(001) substrate. The thicknesses of both layers are chosen to provide the largest overlap of the optical mode and the Er³⁺ doped material at the wavelength of 1540 nm. This was done by optimizing the electric field intensity resulting from the counter-propagating fields after a single reflection at the *a*-SiO_x(Er)/air – (E_{air}) and the *a*-SiO_x(Er)/SiO₂ – (E_{SiO_2}) interfaces in all points of the *a*-SiO_x(Er) layer. In other words, we have optimized the integral

$$\Gamma = (1/L) \int_0^L |E_{\text{air}}(x) + E_{\text{SiO}_2}(x)|^2 dx \quad (1)$$

at the 1540 nm wavelength, where L is cavity length. This approach is valid for small Q-factor structures and optimizes the modal effective volume within the *a*-SiO_x(Er). However, as it will be shown later, we also need to consider the higher Q-factor modes that exist in the 800–1000 nm wavelength range. We show that the resonances within this range enhances the optical emission by over two times and, as a consequence, they enhance the emission at 1540 nm by over four times due to the cross pumping mechanism. After annealing optimization, we obtain a further five times increase in the emission at 1540 nm, as compared with the as-deposited sample.

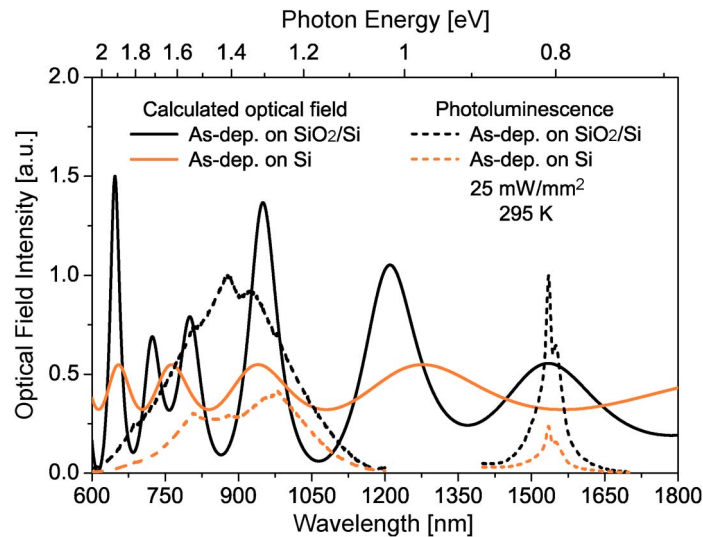


Fig. 1. PL spectra at 295 K in the 600–1200 nm and 1400–1700 nm wavelength ranges of $a\text{-SiO}_x\langle\text{Er}\rangle$ layers as-deposited on (530 nm) SiO_2/Si and on Si, in contrast with the calculated optical field intensity inside the $a\text{-SiO}_x\langle\text{Er}\rangle$ layer for structures with and without the SiO_2 film.

2. Experimental Details

An n -type Czochralski Si (001) wafer (thickness 500 μm) was used as starting material in the samples synthesis. A 530 nm thermal oxide layer (SiO_2) was obtained by wet oxidation of Si wafer at 1000 $^\circ\text{C}$ for 270 min. in a flux of 1.0 l/min of O_2 and water vapor. Subsequently, a 600 nm thick $a\text{-SiO}_x\langle\text{Er}\rangle$ film was deposited on this SiO_2/Si substrate by reactive co-sputtering deposition. The heterostructure proposed here leads to an optimized overlap between the optical field and the active region, thus the largest integral Γ at 1540 nm, as described by Figueira *et al.* [17]. Rutherford Backscattering Spectrometry (RBS) indicated an erbium concentration of ~ 0.01 at.% and an oxygen concentration of ~ 7.8 at.%. After deposition, the sample was cleaved in two pieces. One piece was thermally annealed at 400 $^\circ\text{C}$ for 1 hour and the other piece at 1150 $^\circ\text{C}$ for 1 hour, both in a N_2 atmosphere (3.0 l/min flux) in order to investigate the light emission evolution. A 600 nm thick $a\text{-SiO}_x\langle\text{Er}\rangle$ film was also deposited directly on Si(001) substrate to allow a comparison with the resonant structure. Photoluminescence (PL) spectroscopy was carried out at room temperature and at low temperatures in a continuous flow variable-temperature He cryostat. We used a 532 nm line of a Solid State Laser as the photoexcitation source. The laser spot area was ~ 1 mm^2 . The PL was dispersed by a single-grating monochromator (SPEX 0.5 m focal length with 600 l/mm grating and 32 $\text{\AA}/\text{mm}$ resolution) and detected by a photomultiplier S1 Hamamatsu (600–1200 nm spectral region) and by a Ge $p\text{-i-n}$ photodiode North Coast (1400–1700 nm wavelength range). Both photodetectors were cooled with liquid nitrogen.

3. Results and Discussion

Fig. 1 shows the PL spectra in the aforementioned wavelength ranges for $a\text{-SiO}_x\langle\text{Er}\rangle$ layers as-deposited on (530 nm) SiO_2/Si and directly on Si substrate. These measurements were performed with an estimated excitation power density of 25 mW/mm^2 . The PL spectra were normalized to the maximum intensity at both ranges. The emission intensity is clearly enhanced for the samples with the SiO_2 layer. More specifically, a twofold enhancement is observed in the 800–1000 nm range while a fourfold enhancement is observed at ~ 1540 nm. Fig. 1 also shows the calculated optical field intensity after infinite roundtrips as a function of wavelength at any arbitrary point inside the $a\text{-SiO}_x\langle\text{Er}\rangle$ layer for samples with and without the SiO_2 film. The optical field intensity is obtained by assuming that the active layer is a Fabry–Perot cavity with length equal to its thickness and with mirrors provided by the top and bottom subsequent interfaces. The field amplitude is obtained by an

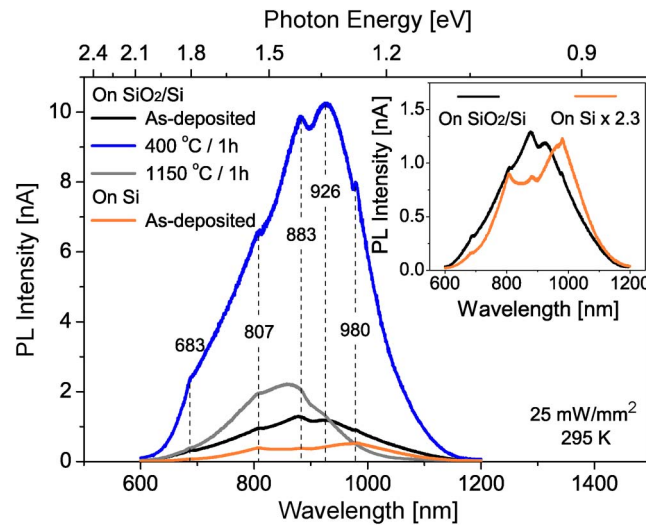


Fig. 2. PL spectra at 295 K in the visible–near infrared region (600–1200 nm) for the samples: as-deposited on Si, as-deposited on SiO_2/Si , and after two different thermal treatment temperatures. The inset shows a twofold enhancement of PL intensity due to the SiO_2 resonant layer.

infinite summation of the multiple reflections from both interfaces for light generated at any given point inside the cavity. The wavelength dependent mirror reflectivity is obtained using a simple transfer matrix method [22]. The Si wavelength dependent refractive index used in the simulation was based on data from references [23], [24]. For the $a\text{-SiO}_x\langle\text{Er}\rangle$ active material, an offset was added to the Si refractive index value such that it asymptotically converges to an index of refraction of 2.6 at 1540 nm as measured by spectroscopic ellipsometry. A refractive index of 1.48 was used for the thermal oxide layer.

The sample with the SiO_2 layer has resonances near 800 nm and 950 nm with Q-factor of ~ 13 and ~ 17 , respectively. A resonance with small Q-factor, $Q \sim 3.5$, is observed at 1535 nm. The sample without the SiO_2 layer has only small Q-factor resonances, $Q \sim 3.5$, near 760 nm and 940 nm.

A close inspection of the optical emission in the 600–1200 nm wavelength range reveals interesting features. Peaks approximately at 683, 807, 883 and 980 nm are observed for both samples with and without the SiO_2 layer (better visualized in the inset of Fig. 2). The peak at ~ 926 nm is only observed for the sample with the SiO_2 layer. Therefore, this peak is most probably related to the multilayer resonance, particularly, to the calculated resonance near 950 nm as described above. On the other hand, the peaks at ~ 683 and ~ 883 nm can be attributed to radiative recombination at localized tail states. Their energy positions depend on the x fraction of oxygen in the $a\text{-SiO}_x$ matrix [25]. Also, it has been reported the possibility that $a\text{-Si}$ -rich clusters and $a\text{-SiO}_2$ grains existent in an $a\text{-SiO}_x$ matrix may cause the emission at these wavelengths [25]. The fact that the Q-factor is small, and has a large linewidth, may lead to some enhancement of the emission at 883 nm. Finally, the peaks at ~ 807 and ~ 980 nm may be assigned, in principle, to the intrinsic Er 4f shell emission ($^4I_{9/2}$ to $^4I_{15/2}$ and $^4I_{11/2}$ to $^4I_{15/2}$, respectively). In particular, the spectral feature at 980 nm was also observed in a similar matrix [9]. However, care must be taken before PL at ~ 807 and ~ 980 nm can definitively be attributed to Er^{3+} . This issue will be discussed later.

We proceed to investigate further improvements in the emission efficiency with the use of thermal treatment on the samples with the SiO_2 resonant structure. Fig. 2 shows the PL spectra taken at 295 K in the 600–1200 nm wavelength range after annealing for 1 hour at 400 °C and at 1150 °C. We kept the spectra for the as-deposited on Si sample for comparison. After annealing at 400 °C there is over eight times increase in PL intensity with respect to the as-deposited sample. In addition, the spectral emission line-shape and the peaks position characteristic of the as-deposited sample remain apparently not affected upon this thermal treatment. On the other hand, after annealing at 1150 °C, the PL intensity shows expressive reduction. Moreover, the PL line-shape and peaks feature

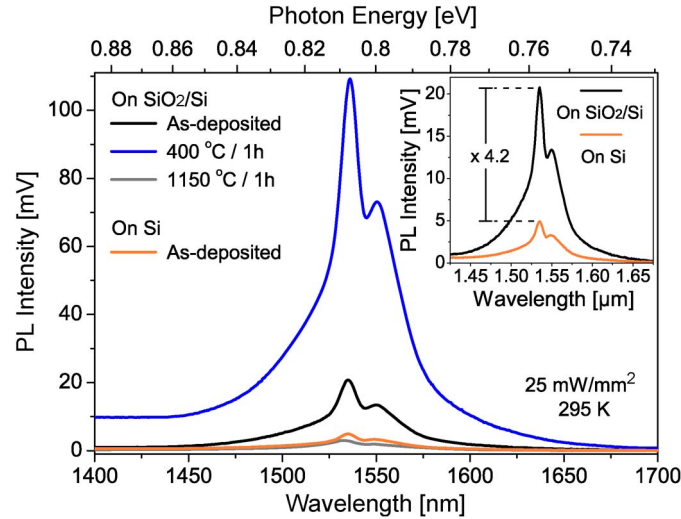


Fig. 3. PL spectra at 295 K in the near-infrared region (1400–1700 nm) for the samples: as-deposited on Si, as-deposited on SiO₂/Si, and after thermal annealing at 400 °C and at 1150 °C both for 1 h. The inset shows a PL enhancement of over four times due to the SiO₂ resonant layer.

change considerably. It is worth observing that after annealing at 1150 °C, the peak at ~980 nm is totally suppressed while the peak at ~807 nm remains. Upon high temperature annealing, silicon segregates forming clusters and there is great healing of the defects generated by the oxygen vacancy dangling bonds. Therefore, we expect that most of the defect-related processes, such as the Er³⁺ resonant pumping and the defect-related emission, should be greatly decreased. This can explain the large overall reduction of the PL. Furthermore, we believe the 980 nm peak arises from the Er³⁺ ⁴I_{11/2} – ⁴I_{15/2} transition and the 807 nm peak is probably generated by some localized radiative defects and coincidentally have similar energy than the ⁴I_{9/2} – ⁴I_{15/2} transition.

Fig. 3 shows the PL spectra in the 1400–1700 nm wavelength range for the four samples: a-SiO_x(Er) layer as-deposited on Si, as-deposited on SiO₂/Si and after two different thermal treatment temperatures, 400 °C/1 h and 1150 °C/1 h. The main peak (highest-intensity at ~1540 nm) corresponds to the ⁴I_{13/2} – ⁴I_{15/2} transition and the second peak at ~1550 nm is caused by the Stark effect [12]. The spectra corresponding to the as-deposited on SiO₂/Si sample also present a substantial enhancement in the emission (about 4 times—see inset of Fig. 3) with respect to the as-deposited on Si sample. This enhancement in the PL caused by the multilayer structure, can be qualitatively explained considering a system with internal spontaneous/stimulated emission generation coupled to several modes with different cavity Q's. Using a simple model based on rate equations, the emission power out of the system at a given mode ω_j can be evaluated by [26]

$$R_i = \frac{\beta_i R_{sp} \hbar \omega_j}{(A - B) Q_{ci} / \omega_j + 1} \quad (2)$$

where A and B are the scattering loss and the stimulated emission rates per photon, respectively. Q_{ci} and β_i are the cold cavity Q and the spontaneous emission factor for the i th mode. R_{sp} is the total spontaneous emission rate. At transparency, $A = B$, the emission is not affected by the different Q's and only modulated by R_{sp} and β_i . For $A > B$, modes with smaller cold cavity Q should have higher emission power. Essentially, lower Q-factor means that light generated within the system is not confined and is readily emitted. In the other hand, only if $A < B$, the higher cold cavity Q emission should be enhanced. In other words, in this last case, the higher cold cavity Q allows a photonic density build up that compensates its higher confinement. This explains the twofold higher emission near 926 nm for the as-deposited on SiO₂/Si sample (inset Fig. 2) only if stimulated emission occurs. The stimulated emission may occur for the defect-related emission and/or for the Er³⁺ ⁴I_{11/2} – ⁴I_{15/2}

transition at 980 nm. However, since $^4I_{11/2}$ quickly decays to $^4I_{13/2}$ level there could be a cross-pumping at 1540 nm. Both the large mode overlap and the low Q-factor at this wavelength lead to a large photon escape from the cavity. In summary, the larger than expected enhancement of the emission at 1540 nm may be explained by the low Q-factor at this wavelength, allowing high external quantum efficiency combined with a higher internal emission rate from the more confined resonance at 980 nm.

We also observed a PL enhancement in the near infrared (NIR) region of over five times after thermal treatment of the as-deposited on SiO₂/Si sample at 400 °C/1 h. This result suggests that a larger fraction of the Er atoms reacts with oxygen during annealing (Er oxidation) forming a greater amount of Er-O optically active complexes [27]. Moreover, it may suggest that there is a higher effective defects density (dangling bonds) that acts as Er luminescence sensitizers. It was showed that any defect due to excess Si in silicon oxide may act as a sensitizer [16]. On the other hand, high temperature annealing leads to a drastic deterioration in the NIR emission efficiency, that is, the Er³⁺ pumping was highly suppressed. The severe decrease observed in PL intensity could be understood as the contribution of two effects: i) decrease of the Er³⁺ excitation rate, and/or ii) lower density of optically active Er³⁺ centers as a result of the local and surrounding environment of the Er ions.

The decrease of the Er³⁺ excitation rate is due to a reduction of the density of sensitizers with the increase of temperature. This reduction can be detected by PL spectra obtained in the visible–near infrared range (Fig. 2), where there is a drastic reduction of emission from a-SiO_x defect-related radiative centers after annealing at 1150 °C/1 h—considering that either the excitation of these centers is mediated by dangling bonds or they themselves emit. Accordingly, the annealing at high temperature should produce a rearrangement and/or a partial annihilation of the dangling bonds leading to a decrease of the Er³⁺ excitation rate too. Indeed, we notice that the PL [1150 °C]/[400 °C] ratio at 600–1200 nm range is about 0.22, while at the 1400–1700 nm range is about 0.027. This indicates that there is not only a decrease in the density of the sensitizers, but also a decrease in the number of optically active Er³⁺ centers. It is known that the PL intensity crucially depends on the Er incorporation conditions on the host matrix, since the Er³⁺ transition probability is determined by the local environment of the ions—more specifically determined by the magnitude of the crystal field which depends on the Er³⁺ sites symmetry (centrosymmetric or noncentrosymmetric lattices) [28]. The luminescence efficiency has been associated to an Er local environment very similar to that of Er₂O₃ where the Er sits in a sixfold coordinated cage (each Er is coordinated by six oxygen atoms), which provides a noncentrosymmetric environment [29], [30]. Tessler *et al.* investigated the possible Er lattice sites and their evolution upon thermal annealing (up to 1100 °C) in samples with an amount of oxygen atoms similar to ours [27], [31]. They observed that the erbium first neighbor shell consists always of oxygen atoms and does not change under annealing. The erbium chemical environment evolves with temperature from a characteristic ErO₃ threefold coordinated oxygen shell toward the Er₂O₃-like sixfold coordinated shell (where the threefold Er coordination has a lower symmetry than the sixfold coordination). Although this increase of coordination with annealing temperature (the Er³⁺ sites become more symmetric) gives rise to a decrease of the transition probability, the main consequence is Er ions surrounding structural change. It was reported that in Er-doped silicon-rich silicon oxide matrix containing Si-NC's, Er³⁺ can exist in two types of centers: isolated or strongly coupled to defects [16]. For the case of isolated centers the emission efficiency of Er³⁺ is significantly limited by distance-dependent energy transfer, which corroborates the results at higher temperature.

In order to make a more meaningful distinction between the types of centers aforementioned, we have investigated the variation of emission intensity of the Er-O complexes with temperature. The temperature dependence of the integrated PL intensity for the annealed samples at 400 °C and at 1150 °C (from now on labeled as S1 and S2, respectively) as a function of the inverse temperature ($1/k_B T$) is depicted in Fig. 4. The data were taken at temperatures ranging from 10 to 295 K at a constant pump power of 45 mW/mm² and normalized with respect to the higher PL intensity. Different PL behaviors with temperature were observed. The PL intensity declines more rapidly up to 70 K for the S2 sample, above which, a much stronger quenching for both samples occurs.

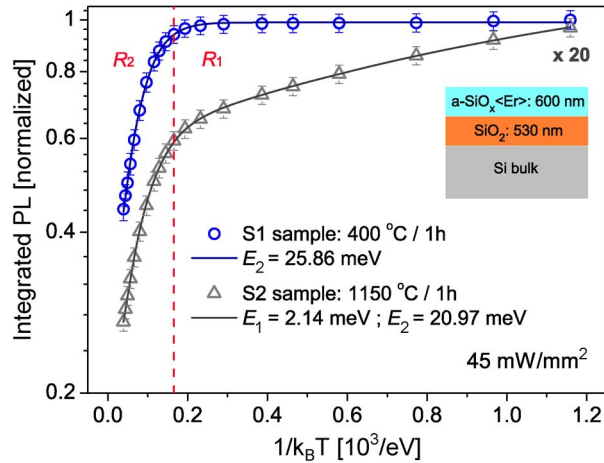


Fig. 4. Arrhenius plot of the integrated PL intensity as a function of $1/k_B T$. The symbols represent the experimental data, while the continuous lines are the theoretical fits according to (3).

TABLE 1

PL parameters obtained from temperature dependence of the integrated PL intensities

Sample	C_1	E_1 (meV)	C_2	E_2 (meV)	R_1	R_2
S1 - 400 °C / 1h	-	-	3.7	25.86	0.94	0.47
S2 - 1150 °C / 1h	1.18	2.14	5.83	20.97	0.61	0.46

Based on the model of the nonradiative recombination, the thermal quenching properties were quantified and analyzed, assuming characteristic thermally deactivated excitation processes, where the temperature dependence of integrated PL intensity $I_{PL}(T)$ is given by [32]

$$I_{PL}(T) = I_0 / \left[1 + \sum_{i=1}^n C_i \exp(-E_i/k_B T) \right] \quad (3)$$

where C_i are the coefficients associated to the thermal dissociation processes of Er centers with deactivation energy E_i , I_0 is the PL intensity at a temperature close to absolute zero and k_B is the Boltzmann constant. $I_{PL}(T)$ is obtained by fitting Gaussian function on the main peak at ~ 1540 nm. The fitting results of the experimental data according to equation (3) are represented in Fig. 4 by continuous lines. For the S1 sample the quenching process is well described by only one regime (solely a deactivation energy $E_2 \sim 26$ meV) while that for the S2 sample two quenching regimes (with deactivation energy $E_1 \sim 2$ meV and $E_2 \sim 21$ meV) are clearly observed. The fitting parameters used to model temperature-dependent Er-PL behavior are presented in Table 1, as well as the ratio R of the integrated PL intensity for two quenching ranges: $R_1 = [I_{PL} - 70 \text{ K}] / [I_{PL} - 10 \text{ K}]$ and $R_2 = [I_{PL} - 295 \text{ K}] / [I_{PL} - 70 \text{ K}]$.

Supposing that the thermal ionization of [Er center—dangling bond defect] pair before the electronic excitation transfer process occurs is dominant on backtransfer mechanism (multiphonon nonradiatives processes) [7], it is reasonable to assume that such energies are associated to Er center—dangling bond decoupling. Remembering that for an effective energy transfer to the 4f electrons either by DRAE process (capture of an electron by dangling bonds) or by resonant dipole-dipole interaction originated by the nonradiative recombination of the electron-hole pairs in the

dangling bonds, it is necessary that the dangling bond be localized nearby the Er-O complexes. Hence, the integrated PL intensity is the response average from Er-O complexes and their vicinity. At lower temperatures ($T < 70$ K), the thermalization energies and the quenching rate values (Table 1) suggest that the deactivated centers of S1 sample differ completely from the S2 sample. Regarding to the latter, possibly photogenerated carriers near weakly coupled centers have less kinetic energy to out diffuse (are more localized) allowing the excitation. In contrast, as temperature increases, the carriers become more delocalized and the quench is very effective for those centers. At higher temperatures ($T > 70$ K), the Er centers for the two samples differ slightly (similar deactivation energies and quenching ratio), apparently due to a small difference in the local order and surrounding of the Er atoms. However, the integrated PL intensity of S2 sample is about 97% lower than S1 sample, which reveals a lower density of optically active Er^{3+} centers. At this point, we also speculate that the annealing at higher temperatures induced some matrix phase separation, or even further Er precipitation that may promote the reduction of active centers.

4. Conclusion

In summary, we have fabricated highly luminescent samples with erbium-doped amorphous silicon suboxide ($a\text{-SiO}_x\langle\text{Er}\rangle$) layers deposited on SiO_2/Si substrates forming a resonator multilayer structure. Twofold improvement in PL intensity of the $a\text{-SiO}_x$ defect-related radiative centers is achieved in the wavelength range between 800 and 1000 nm due to the resonator structure. The PL intensity in the wavelength range between 1500 and 1600 nm (region of $\text{Er}^{3+} {}^4\text{I}_{13/2} - {}^4\text{I}_{15/2}$ transition) is increased four times, apparently due to optical cross-pumping at 980 nm (${}^4\text{I}_{11/2} - {}^4\text{I}_{15/2}$ transition). After temperature annealing optimization, the emission at 1540 nm was further enhanced over five times as compared to the as-deposited sample.

References

- [1] S. G. Cloutier, P. A. Kosyrev, and J. Xu, "Optical gain and stimulated emission in periodic nanopatterned crystalline silicon," *Nat. Mater.*, vol. 4, pp. 887–891, 2005.
- [2] M. A. Green, J. Zhao, A. Wang, P. J. Reece, and M. Gal, "Efficient silicon light-emitting diodes," *Nature*, vol. 412, pp. 805–808, 2001.
- [3] I. D. Rukhlenko, C. Dissanayake, M. Premaratne, and G. P. Agrawal, "Maximization of net optical gain in silicon-waveguide Raman amplifiers," *Opt. Exp.*, vol. 17, no. 7, pp. 5807–5814, Mar. 2009.
- [4] J. Yang and P. Bhattacharya, "Integration of epitaxially-grown InGaAs/GaAs quantum dots lasers with hydrogenated amorphous silicon waveguides on silicon," *Opt. Exp.*, vol. 16, no. 7, pp. 5136–5140, Mar. 2008.
- [5] L. Ferraioli, M. Wang, G. Pucker, D. Navarro-Urrios, N. Daldosso, C. Kompocholis, and L. Pavesi, "Photoluminescence of silicon nanocrystals in silicon oxide," *J. Nanomater.*, vol. 2007, pp. 43 491–43 495, 2007.
- [6] D. R. Solli, P. Koonath, and B. Jalali, "Broadband Raman amplification in silicon," *Appl. Phys. Lett.*, vol. 93, no. 19, pp. 191105-1–191105-3, Nov. 2008.
- [7] W. Fuhs, I. Ulber, G. Weiser, M. S. Bresler, O. B. Gusev, A. N. Kuznetsov, V. K. Kudoyarova, E. I. Terukov, and I. N. Yassievich, "Excitation and temperature quenching of Er-induced luminescence in $a\text{-Si:H(Er)}$," *Phys. Rev. B, Condens. Matter*, vol. 56, no. 15, pp. 9545–9551, Oct. 1997.
- [8] H. Kühne, G. Weiser, E. I. Terukov, A. N. Kusnetsov, and V. Kh. Kudoyarova, "Resonant nonradiative energy transfer to erbium ions in amorphous hydrogenated silicon," *J. Appl. Phys.*, vol. 86, no. 2, pp. 896–901, Jul. 1999.
- [9] A. Janotta, M. Schmitd, R. Janssen, M. Stutzmann, and Ch. Buchal, "Photoluminescence of Er^{3+} -implanted amorphous hydrogenated silicon suboxides," *Phys. Rev. B*, vol. 68, no. 16, pp. 165207-1–165207-17, Oct. 2003.
- [10] R. J. Mears, L. Reekie, I. M. Jauncey, and D. N. Payne, "Low-noise erbium-doped fibre amplifier operating at 1.54 μm ," *Electron. Lett.*, vol. 23, no. 19, pp. 1026–1028, 1987.
- [11] C. A. Millar, I. D. Miller, B. J. Ainslie, S. P. Craig, and J. R. Armitage, "Low-threshold CW operation of an erbium-doped fibre laser pumped at 807 nm wavelength," *Electron. Lett.*, vol. 23, no. 16, pp. 865–866, Jul. 1987.
- [12] E. Desurvire, *Erbium Doped Fiber Amplifiers*. New York: Wiley, 1994, pp. 207–306.
- [13] P. G. Kik and A. Polman, "Exciton-erbium interactions in Si nanocrystal-doped SiO_2 ," *J. Appl. Phys.*, vol. 88, no. 4, pp. 1992–1998, Aug. 2000.
- [14] M. Fujii, M. Yoshida, Y. Kanzawa, S. Hayashi, and K. Yamamoto, "1.54 μm photoluminescence of Er^{3+} doped into SiO_2 films containing Si nanocrystals: Evidence for energy transfer from Si Nanocrystals to Er^{3+} ," *Appl. Phys. Lett.*, vol. 71, no. 9, pp. 1198–1200, Sep. 1997.
- [15] P. G. Kik, M. L. Brongersma, and A. Polman, "Strong exciton-erbium coupling in Si nanocrystal-doped SiO_2 ," *Appl. Phys. Lett.*, vol. 76, no. 17, pp. 2325–2327, Apr. 2000.
- [16] D. Kuritsyn, A. Kozanecki, H. Przybylińska, and W. Jantsch, "Defect-mediated and resonant optical excitation of Er^{3+} ions in silicon-rich silicon dioxide," *Appl. Phys. Lett.*, vol. 83, no. 20, pp. 4160–4162, Nov. 2003.

- [17] D. S. L. Figueira, D. Mustafa, L. R. Tessler, and N. C. Frateschi, "Resonant structures based on amorphous silicon suboxide doped with Er³⁺ with silicon nanoclusters for an efficient emission at 1550 nm," *J. Vac. Sci. Technol. B, Microelectron. Nanometer Struct.*, vol. 27, no. 6, pp. L38–L41, Nov. 2009.
- [18] C. Creatore and L. C. Andreani, "Quantum theory of spontaneous emission in multilayer dielectric structures," *Phys. Rev. A*, vol. 78, no. 6, pp. 063825-1–063825-15, Dec. 2008.
- [19] R. S. Tummidi, R. M. Pafchek, K. Kangbaek, and T. L. Koch, "Modification of spontaneous emission rates in shallow ridge 8.3 nm Erbium doped silica slot waveguides," in *Proc. 6th IEEE GFP*, 2009, pp. 226–228.
- [20] H. Zhao, J. Zhang, G. Liu, and N. Tansu, "Surface plasmon dispersion engineering via double-metallic Au/Ag layers for II-nitride based light-emitting diodes," *Appl. Phys. Lett.*, vol. 98, no. 15, pp. 151115-1–151115-3, Apr. 2011.
- [21] C.-H. Lu, C.-C. Lan, Y.-L. Lai, Y.-L. Li, and C.-P. Liu, "Enhancement of green emission from InGaN/GaN multiple quantum wells via coupling to surface plasmons in a two-dimensional silver array," *Adv. Funct. Mater.*, vol. 21, no. 24, pp. 4719–4723, Dec. 2011.
- [22] E. K. Sharma, A. K. Ghatak, and I. C. Goyal, "Matrix method for determining propagation characteristics of optical waveguides," *IEEE J. Quantum Electron.*, vol. QE-19, no. 8, pp. 1231–1233, Aug. 1983.
- [23] M. A. Green and M. J. Keevers, "Optical properties of intrinsic silicon at 300 K," *Prog. Photovoltaics, Res. Appl.*, vol. 3, no. 3, pp. 189–192, 1995.
- [24] H. R. Philipp and E. A. Taft, "Optical constants of silicon in the region 1 to 10 eV," *Phys. Rev.*, vol. 120, no. 1, pp. 37–38, Oct. 1960.
- [25] K. Yoshida, I. Umezu, N. Sakamoto, M. Inada, and A. Sugimura, "Effect of structure on radiative recombination processes in amorphous silicon suboxide prepared by rf sputtering," *J. Appl. Phys.*, vol. 92, no. 10, pp. 5936–5941, Nov. 2002.
- [26] G. P. Agrawal and N. K. Dutta, *Semiconductor Lasers*, 2nd ed. New York: Van Nostrand Reinhold, 1993.
- [27] L. R. Tessler, C. Piamonteze, M. C. Martins Alves, and H. Tolentino, "Evolution of the Er environment in a-Si:H under annealing: Ion implantation versus co-deposition," *J. Non-Cryst. Solids*, vol. 266–269, pp. 598–602, May 2000.
- [28] B. R. Judd, "Optical absorption intensities of rare-earth ions," *Phys. Rev.*, vol. 127, no. 3, pp. 750–761, 1962.
- [29] D. L. Adler, D. C. Jacobson, D. J. Eaglesham, M. A. Marcus, J. L. Benton, J. M. Poate, and P. H. Citrin, "Local structure of 1.54- μm -luminescence Er³⁺ implanted Si," *Appl. Phys. Lett.*, vol. 61, no. 18, pp. 2181–2183, Nov. 1992.
- [30] R. M. Moon, W. C. Koehler, H. R. Child, and L. J. Raubenheimer, "Magnetic structures of Er₂O₃ and Yb₂O₃," *Phys. Rev.*, vol. 176, no. 2, pp. 722–731, Dec. 1968.
- [31] C. Piamonteze, A. C. Iñiguez, L. R. Tessler, M. C. Martins Alves, and H. Tolentino, "Environment of erbium in a-Si:H and a-SiO_x:H," *Phys. Rev. B*, vol. 24, no. 21, pp. 4652–4655, 1998.
- [32] W. Rühle, W. Schmid, R. Meck, N. Stath, J. U. Fischbach, I. Strottner, K. W. Benz, and M. Pilkuhn, "Isoelectronic impurity states in direct-gap III–V compounds: The case of InP:Bi," *Phys. Rev. B*, vol. 18, no. 12, pp. 7022–7032, Dec. 1978.